

WAKE VORTEX RESULTS FROM THE AWIATOR PROJECT

A.C. de Bruin⁺, G. Schrauf^{*}

⁺ NLR, Voorsterweg 31, 8316PR Marknesse, the Netherlands

^{*} Airbus, Airbus Allee 1, 28199 Bremen, Germany

OVERVIEW

Wake turbulence poses a potential hazard to following aircraft. Therefore, minimum aircraft separation distances, based on an aircraft weight classification scheme, are recommended by ICAO in order to assure proper safety during all flight phases. These pose a limiting factor for the capacity at congested airports. If modifications of the wing configuration can be shown to alleviate the strength and fasten the decay of the wake vortices, this potentially allows a mitigation of aircraft separation rules.

The EU co-funded projects EUROWAKE, C-Wake and the wake vortex task of AWIATOR form a continuous line of research focussed on the effects of wing modification on wake roll-up and decay. The EUROWAKE project (1996-1998) concentrated on wake formation and roll-up in the near wake. The C-Wake project (2000-2003) investigated wing span-loading concepts and other wing modifications up to the extended wake region using wind tunnel, towing tank, B10 catapult facility and a limited number of flight tests with the A340-300 in landing configuration, using ground-based LIDAR. The AWIATOR project (2002-2007) focussed on the selection of wake alleviation concepts, to be tested in flight on the same aircraft, also in landing configuration. A down-selection of promising configurations was made from extensive CFD simulations, wind tunnel experiments, free-flying model tests and tests in a large towing tank facility. This paper gives an overview of the methods used for the selection process, the physical mechanisms exploited and the wake alleviation results obtained. Additional information on the AWIATOR project is given in [1-3].

1. AN INTRODUCTION TO WAKE FORMATION AND DECAY

The formation of the wake vortex system behind an aircraft is the direct consequence of generating lift [4, 5]. The wake starts as a vorticity layer shed from the trailing edges of wing and tail. Within a few wingspans downstream, the vorticity sheets roll up into a system of discrete vortices. The merging of these vortices ultimately leads to a single pair of trailing vortices. Their deformation and decay depend on details of the merging process and the level of atmospheric turbulence. The initial circulation strength Γ_0 (the integral of vorticity over the half-wake) is proportional to the total lift (equal to weight W) and inverse proportional to the airspeed V and the lateral spacing b_0 between the vortices (or more precisely: between the vorticity centroids):

$$\Gamma_0 = \frac{W}{\rho V b_0} = \frac{V S C_L}{2 b_0}$$

Herein, ρ is the air density and S is the projected wing surface. The distance b_0 can be designated as sb , where b is the wing span and s is a parameter depending on the

span-loading. For an elliptically loaded wing $s = \pi/4$. If an aircraft flies in high lift configuration, the airspeed is low and the circulation strength is high. When flying at higher altitude with a given lift-coefficient C_L , the air density becomes smaller and the aircraft has to fly faster, so the circulation strength increases. In the absence of vertical wind, the vortices sink due to mutual induction. The initial sink velocity w_0 of the vortex pair is:

$$w_0 = \frac{\Gamma_0}{2\pi sb} = \frac{W}{2\pi \rho V (sb)^2} = \frac{V S C_L}{4\pi (sb)^2}$$

Based on the sink velocity w_0 and distance between the vortices b_0 , a reference time scale t_0 can be defined as:

$$t_0 = \frac{b_0}{w_0} = \frac{4\pi (sb)^3}{V S C_L}$$

These equations show the importance of the wing span loading parameter s for the initial circulation strength Γ_0 (inverse proportional to s), the initial vortex sink speed (inverse proportional to s^2) and the characteristic time scale for vortex decay (proportional to s^3). The final decay of the vortex pair is subject to the atmospheric turbulence and the turbulence and 3D wake deformations resulting from the wake roll-up and merging process.

To enable a comparison of different configurations, reference conditions are taken for an aircraft with an elliptically loaded wing having the same span and lift, i.e. with $s = \pi/4$. This defines the reference circulation strength Γ^* , the reference sink velocity w^* and the reference time t^* . The latter is used to define non-dimensional time $\tau = t/t^*$. Instead of the total circulation Γ , it is more appropriate for LIDAR measurements to use the circulation Γ_{5-15} which is the part of the circulation that is contained in a ring with an inner radius of 5m and an outer radius of 15m (see for example Holzäpfel [6]). A further important parameter is the vortex core radius r_c .

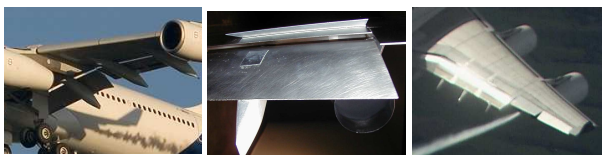
2. TESTED HIGH-LIFT CONFIGURATIONS

In this chapter we give a brief overview on the configurations that were considered in the AWIATOR programme. At the start of the project, several devices were proposed to influence the wake in different ways, some examples are shown in Fig. 1. Subsequent testing early in the project showed that none of these devices was sufficiently promising to justify the extra weight and production costs for full scale application on an aircraft. Therefore, the work was re-focussed on wing span-loading concepts that use existing control surfaces on the A340-300, such as differential spoiler settings (DSSs) or differential flap settings (e.g. DFS 32/10: inboard flap at 32 and outboard flap at 10 deg). During the pre-selection phase a large number of flap settings were considered. For the first flight test it was not possible to use DFS, but two DSSs configurations were designed and tested as an alternative to simulate an inboard loaded flap setting (outboard spoiler #6 deflected 9 deg) and an outboard loaded flap setting (with all spoilers, except spoiler #6,

deflected 3 deg). For the second flight test, an inboard loaded case (DFS 32/10) and a configuration with spoiler #6 deflected at 20 deg were selected. In addition, from advanced numerical simulations using large eddy simulation (LES), a case with +/-10 deg oscillating in- and outboard ailerons was selected. The selected cases for F/T-2 are shown in Fig. 2. No outboard loaded DFS concept has been selected, because quite large values for the inboard counter rotating circulation strength are needed (see e.g. [7]), that are not really manageable on an existing aircraft.



swept plate cylinder "wish-bone"
FIG 1. Devices tested early in the project



DFS 32/10 Spoiler #6 Moving ailerons
FIG 2. Configurations as finally tested

3. SUBSCALE TESTING TECHNIQUES USED

In order to take maximum advantage of available testing techniques and cover the entire range of interest from near wake until about 150 wing spans downstream or more, different testing and calculation techniques were used, as shown in Fig. 3.

Detailed measurements in the near wake region are needed to verify the near wake flow topology and span-loading characteristics. These data were used to initialise temporal CFD simulations for far-wake predictions. Tests in DNW-LST (near wake) and DNW-LLF (extended near wake) wind tunnels were done with a rake with 5-hole probes. Fig. 4 shows the underwater model with through-flow nacelles as tested upside down in DNW-LLF. Fig. 5 shows a vorticity distribution, measured in the very near wake at $x/b=0.03$ in DNW-LST. Fig. 6 shows the excellent reproducibility of the vortex velocity distributions, measured at two different free-stream velocities in the DNW-LLF.

The low speed wind tunnel LSWT at Airbus Bremen was used early in the project for flight clearance aspects. Specific tests for the free-flying model configurations to be tested in the B20 catapult facility were made in the DNW-NWB (see Fig. 4). These tests were made: i) to determine the horizontal tail setting for equilibrium flight; ii) to check flow separation at low Reynolds number high-lift conditions; and iii) to measure near-wake flow fields.

Tests at the Technical University of Munich used a multi-wire hotwire probe to measure unsteady flow phenomena in near and extended near wakes. This enabled the determination of turbulence intensities and even Reynolds shear stress components [8]. Fig. 7 shows a comparison of turbulence intensity distributions at $x/b=2.0$ (span-wise velocity fluctuation component) for the baseline configuration and a configuration with deflected outboard

spoiler. The different vortices are labelled: WTV (wing tip vortex), ONV (outer nacelle vortex), OFV (outer flap vortex) and IFV (inner flap vortex). Clearly the deflected spoiler causes significant extra turbulence in the near wake region and an earlier merging of the outer and inner flap vortex. Spectral analysis of velocity components in the wake of the model with a cylinder device (shown in Fig. 1 and meant to enhance Crow instability) showed no discernable effect on flow unsteadiness at some distance downstream, so no further testing with this device was made.

Extensive cross checking between facilities and measurement techniques was made. Fig. 8 shows e.g. an excellent agreement between three different wind tunnels for the baseline configuration.

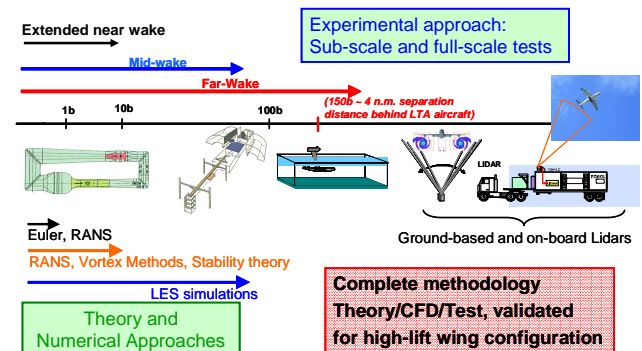


FIG 3. Overview of test techniques and calculation methods, used to cover the range of interest downstream of the wake generating aircraft.

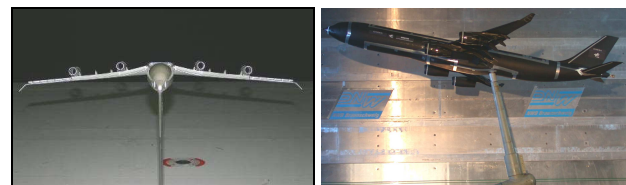


FIG 4. The underwater model in DNW-LLF (left) and the free-flying catapult model in DNW-NWB wind tunnel

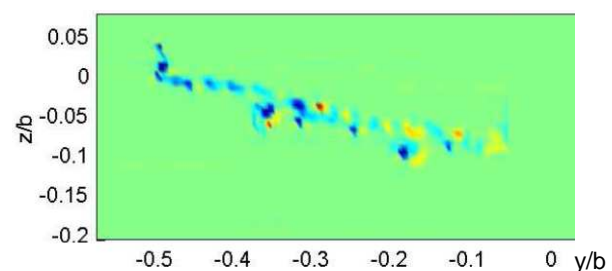


FIG 5. Measured vorticity distribution from 5-hole rake survey at $x/b=0.03$ behind the baseline model in DNW-LST wind tunnel (Airbus).

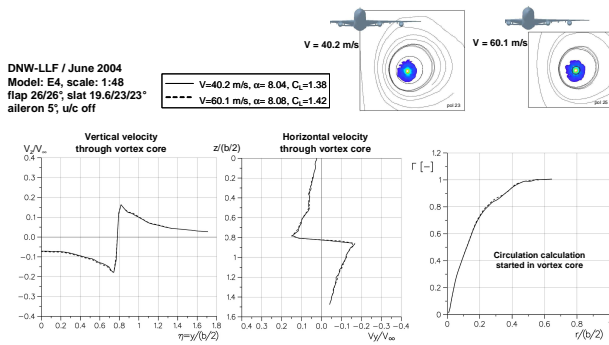


FIG 6. Comparison of wake properties at $x/b = 14.35$ in DNW-LLF wind tunnel, two wind speeds ($V=40$ and 60 m/s), measurements by Airbus.

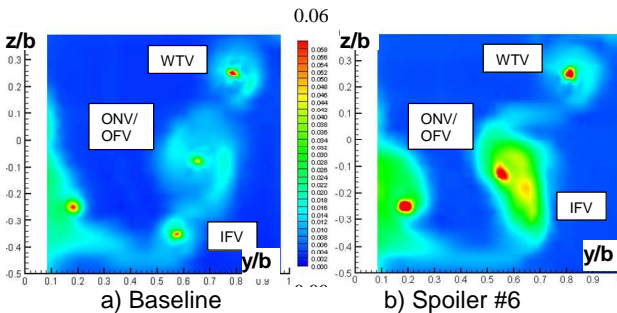


FIG 7. Effect of deflected spoiler on lateral turbulence intensity distribution at $x/b=2$ in wake of the TAK model (hot-wire measurements by TUM-AER).

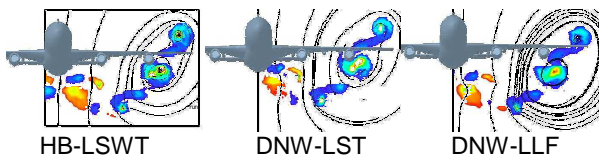


FIG 8. Repeatability of results in different wind tunnels, baseline configuration, $x/b=0.5$ (Airbus).

Due to the insufficient length of wind tunnel test sections, the HSVA towing tank and the ONERA B20 catapult facility were used to measure the wake characteristics further downstream. Each facility has its own advantages and peculiarities and uses different equipment. Therefore both facilities were used complementary throughout the project

The large ONERA B-20 catapult facility was entirely new. The test facility with a free flying model is shown in Fig. 9 and the PIV test set-up, using 12 camera's, is shown in Fig. 10. The first entry showed that the measurements were influenced by so-called "end effects", caused by travelling waves entering the test domain due to start- and stop of the model. With own funding ONERA made large efforts to investigate and cure the problem. At the position of the PIV observation plane, at 11m from the model launching point, the test results are valid until $x/b=30$. High resolution PIV data are obtained, as shown in Fig. 11 for the baseline and DFS 26/10 configuration. ONERA also developed a mini-LIDAR system (see Fig. 12) that provides complementary flow vortex tracking information and can be positioned at any location along the model track. By shifting the LIDAR measuring plane to a location 28 m from the model launching point, the validity range was extended to 80 wingspans (see Fig. 13).

The velocity measurements from the mini-LIDAR can be compared with those measured during flight tests [9]. As shown in Fig. 14 a very good correlation is found. However, the velocity peaks found with mini-LIDAR are somewhat larger than those observed in the flight tests.

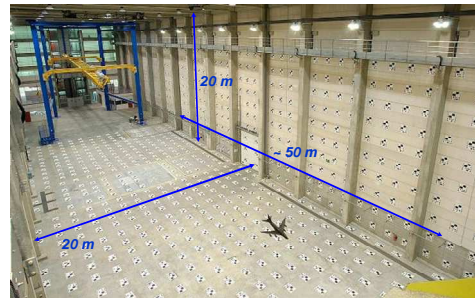


FIG 9. ONERA B-20 catapult facility with free flying model

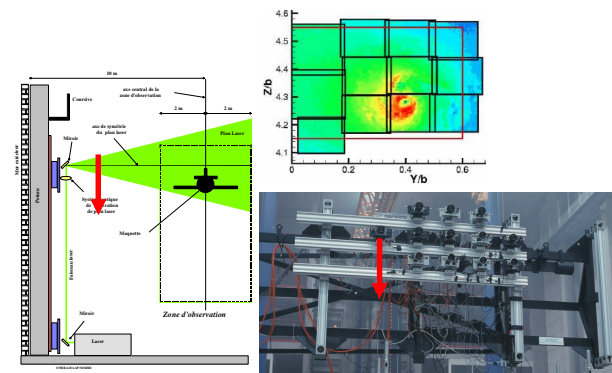


FIG 10. Laser sheet and PIV system with 12 overlapping camera's in ONERA B-20 catapult facility. Both slowly traversed with the sinking wake.

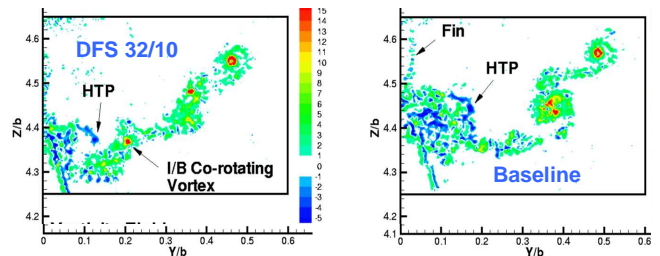


FIG 11. Detailed vorticity fields at $x/b=1.3$, from ONERA B-20 catapult tests with 12 PIV cameras (ONERA & DLR).

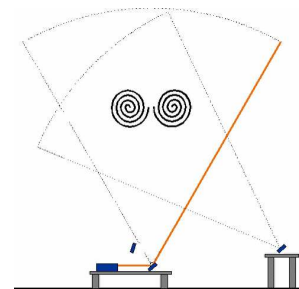


FIG 12: Mini-LIDAR tracking technique with two simultaneously rotating mirrors, as developed by ONERA for the B-20 catapult facility.

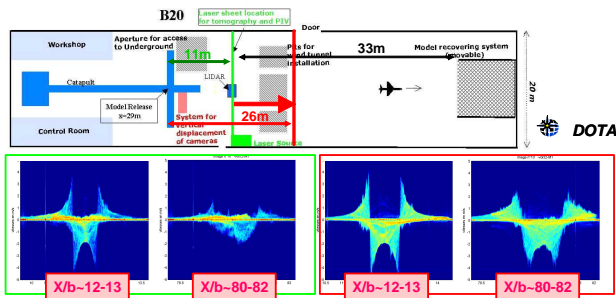


FIG 13. Improved mini-LIDAR signal by shifting the LIDAR plane further from model launch point (ONERA).

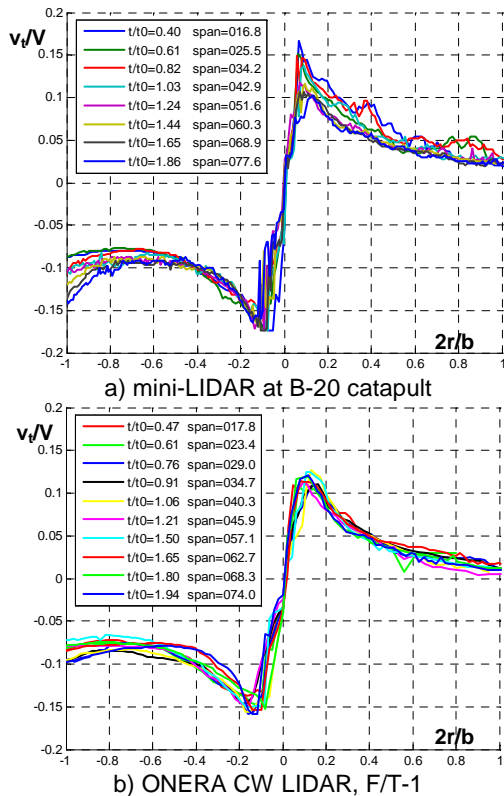
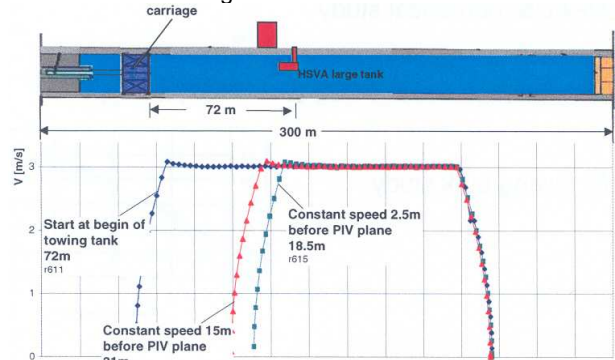


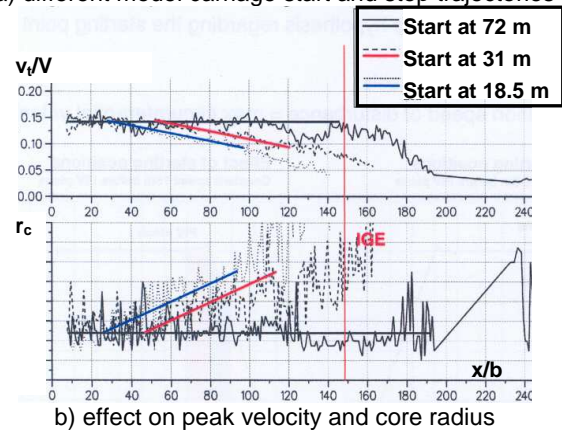
FIG 14. Comparison of B20 and F/T-1 LIDAR measurements by ONERA, between $x/b=17$ and 80 .

The HSVA towing tank facility is 300 m long, 18 m wide and 6 m deep. The model support sting, mounted to the upper side of the fuselage, is connected to a model carriage. The model is accelerated up to 2.5 m/s, passes a pulsed laser light screen and is stopped sufficiently far behind it, so that end effects are avoided. The vertical temperature gradient in the water basin was monitored in order to assure that thermal stratification was sufficiently low. Dedicated tests for end effects (Fig. 15) and with different depths of the model (Fig. 16), confirmed that, with proper model acceleration strategy, the depth of the basin becomes the limiting factor. For the finally selected model depth of one wing span the vortices come into ground effect at about $x/b=150$. A single high resolution PIV recording camera was used in the towing tank. Fig. 17 shows a good agreement between DNW-LLF wind tunnel (5-hole rake) and towing tank data (PIV). The scatter in PIV images represents temporal fluctuations which are smoothed out by the long measuring time of the five-hole probe. From the PIV data it is possible to

determine the decay of the maximum tangential velocity and the development of core radius. Fig. 18 shows, as an example, the favourable effect of a deflected outboard spoiler on maximum tangential velocity (reduced) and core radius (increased). Fig. 19 shows a compilation of towing tank results for baseline, deflected outboard spoiler and DFS 32/10 configuration.



a) different model carriage start and stop trajectories



b) effect on peak velocity and core radius
FIG 15. End-effect investigation by Airbus in HSVA towing tank.

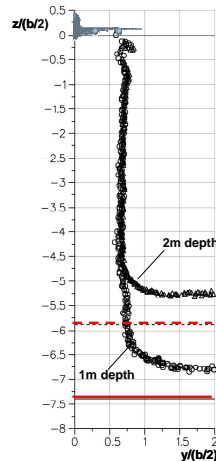


FIG 16. Influence of model depth on vortex sinking (subject to ground effect) in HSVA towing tank (Airbus measurements)

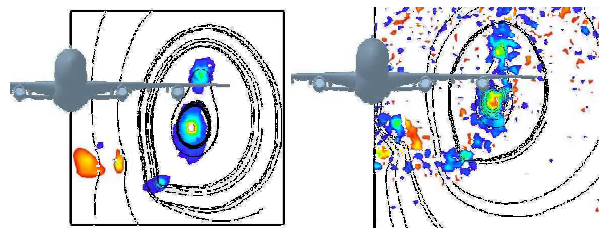


FIG 17. Repeatability between DNW-LLF (5-hole probe) and HSVA (PIV), baseline configuration at $x/b=2$ (Airbus).

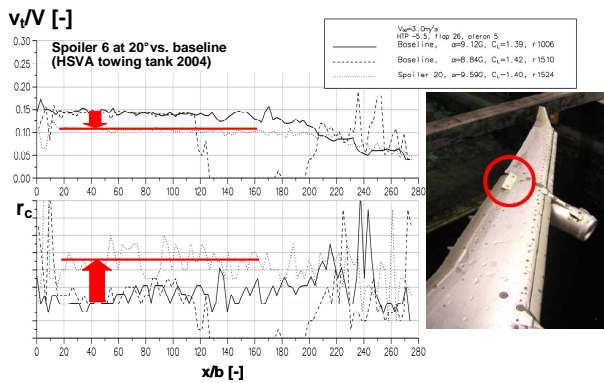


FIG 18. Effect of spoiler #6 on maximum tangential velocity and core radius, HSVA towing tank tests (Airbus)

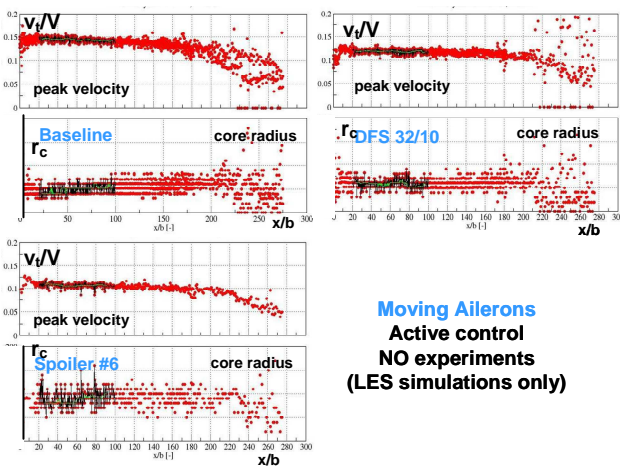


FIG 19. Peak velocity and core radius for F/T-2 configurations, as evaluated from HSVA tests (Airbus).

4. THE USE OF ADVANCED NUMERICAL SIMULATION METHODS

For selecting interesting span-loading concepts, the prediction of wing span-loading and subsequent wake roll-up and merging is of prime importance. Different methods based on either quick (lifting surface method with viscous coupling of ONERA, followed by 2D viscous roll-up simulations by UCL) or slow (e.g. RANS simulations by DLR) methods were applied. With the quick method a large number of DFS settings were considered and linear stability characteristics were evaluated by ONERA. This showed larger instability growth rates for outboard loaded configurations like DFS 17/32 and DFS IN/26. So some of these cases were further tested, but in the final flight tests outboard loaded configurations could not be tested.

The near wake of the complex A340 high-lift configuration was computed with RANS, using the DLR-TAU method and various turbulence models. Span-loading and near wake characteristics were computed (using up to 16 million grid points). Results for the baseline configuration are shown in Fig. 20. From comparison of the RANS and experimental data it was clear that, despite the large number of grid points, RANS becomes too diffusive and dissipative further downstream. However, RANS simulations provide more realistic near wake data than lifting surface methods and can thus be used in a wake simulation strategy starting from the aircraft geometry.

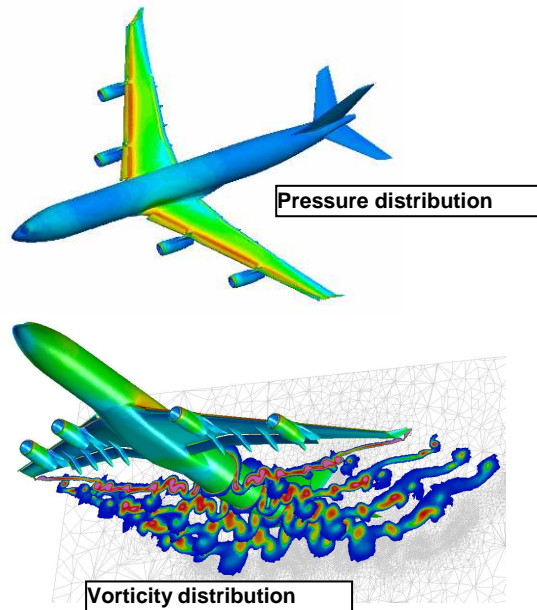


FIG 20. Computed pressure and vorticity distributions in the near wake (RANS simulation with DLR-TAU code until $x/b=0.85$).

At the beginning of the project a benchmark temporal LES simulation of a 4-vortex case ($\Gamma_2/\Gamma_1=-0.3$, $b_2/b_1=0.3$, $r_{c,2}/r_{c,1}=2/3$, sub-fix 1 refers to the main outboard and sub-fix 2 to the counter-signed inboard vortex) was performed by UCL, CERFACS and DLR, using four different numerical codes. The length of the computational box was limited to one wavelength of the most unstable instability mode ($\lambda=0.983b_1$) and a small initial amplitude for that mode was described. CERFACS used a 6th order finite difference method with a filtered structure function sub-grid model. DLR used a 2nd order finite difference method with a modified Smagorinsky model. UCL used a spectral method and a vortex-in-cell (VIC) method with a multi-scale sub-grid model. A quasi-Euler approach ($1/Re=0$) was used in all simulations, i.e. a LES simulation with only the sub-grid scale model. Fig. 21 indicates that all methods predict a very similar growth of modal energy for the prime and even the first harmonic disturbance mode. The 2nd order method displays some decay of energy from the start, as if the simulation runs for an effective Reynolds number. Here the NaCoo modification of the Smagorinsky model shows some improvement. Yet, all models predict a very similar rapid decay onset time. An example of the computed vorticity field at later stages of vortex interaction (UCL calculation with spectral method at $\tau^*=0.86$) is shown in Fig. 22. Later three-dimensional temporal LES simulations, starting from near wake measured data, were made by CERFACS and UCL to support the selection of configurations. Results from UCL, for the situation after merging and roll-up of the vortices (at about non-dimensional time $\tau^*=0.65$), are shown in Fig. 23. From these simulations it was concluded that differences in the vortex merging process create differences in the flow turbulence around the vortices that might have an effect on the later decay. 2D and 3D LES simulations by CERFACS reveal a rapid change of core size at the moment of vortex merging, a slow growth in the other phases and a two-length scale vortex core structure after merging (an inner $r^{-0.45}$ and an outer r^{-1} scaling). An example for the DFS 32/10 case is shown in Fig. 24.

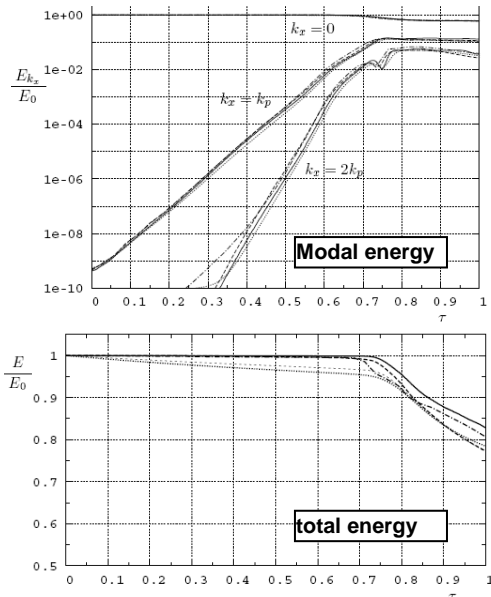


FIG 21. Benchmark case with 4 different codes: SM (UCL, solid line), FD6 (CERFACS, dash), FD2 (DLR, dot): Smagorinsky; light dash: NaCoo) and VIC (UCL, dash-dot).



FIG 22. Benchmark calculation result for spectral method of UCL, at later stage of vortex interaction ($\tau^*=0.86$).

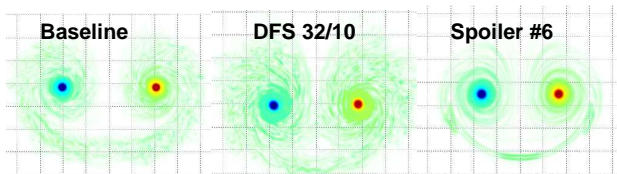
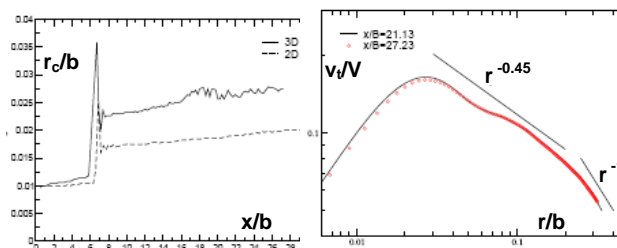


FIG 23. Vorticity distributions (averaged along length of computational box) from LES simulations with pseudo-spectral method of UCL.



a) core growth b) core structure
FIG 24. 2D and 3D LES results for DFS 32/10 case, showing core size growth r_c/b as function of x/b and v_t/V as function of distance to core r/b (CERFACS).

Two temporal LES were made by UCL with the in- and outboard ailerons oscillating in anti-phase (± 10 deg amplitude at 0.2 Hz) and an additional simulation for the non-oscillating baseline case was made for reference. The simulations were made in a 6.9 wingspan (one Crow wave-length) long computational box. The VIC method used required up to 40 million grid points at the end of the simulations. Initial conditions for one wave-length were specified from estimated span-loadings at ± 10 , zero and -10 deg deflection of the ailerons. Two different span-loading assumptions were tried. Both showed a significantly enhanced Crow mode. Fig. 25 shows the initial vorticity field in the computational box with the initial conditions defined Airbus. The computed evolution of modal energy with- and without moving ailerons and the slow growth rate of the Crow mode as predicted by stability theory (the red line) are also shown in Fig. 25. The simulations show that in calm air conditions (a worst case scenario for wake encounters) periodic oscillating ailerons could enhance Crow instability. Therefore, this configuration was also selected for the second flight test.

Temporal LES simulations by DLR concentrated on the impact of atmospheric turbulence on wake decay (see also [10]). First a simulation until well developed turbulence was made and then the vortices were released into an $8b_0$ long computational box. Fig. 26 shows, for the baseline configuration, the predicted circulation decay for eddy dissipation rate level $\varepsilon=10^{-3} \text{ m}^2\text{s}^{-3}$. The symbols reflect the large variation in circulation strength that can be found in cross planes of the computation box at a given time instant (as shown in Fig. 27). These simulation results, contributed much to the understanding of the observed scatter in LIDAR data, as measured during the flight tests in realistic atmospheric turbulence conditions.

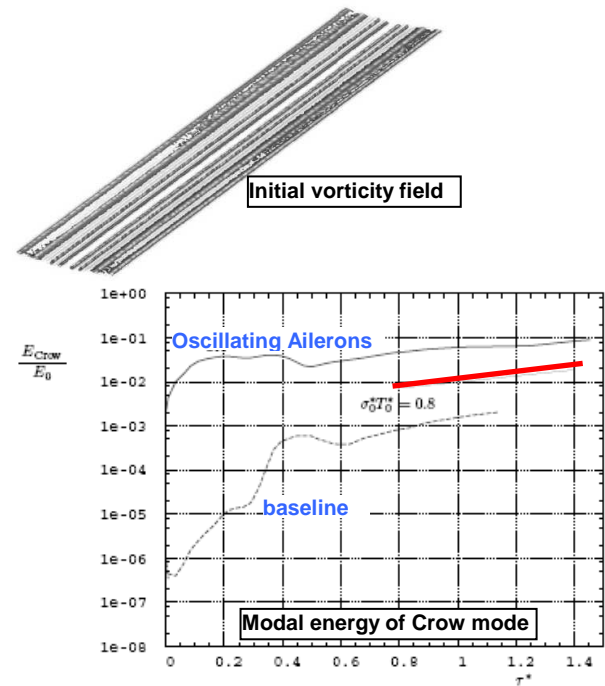


FIG 25. LES simulation of the periodic forced Crow mode by moving ailerons (UCL, using initial span loading distributions from Airbus)

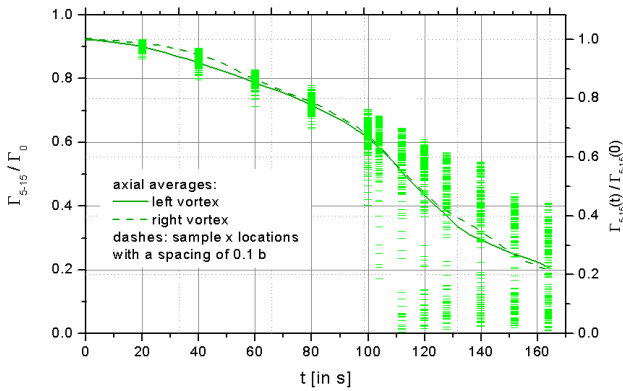


FIG 26. LES of circulation decay, at various time instants, in realistic turbulence conditions: $\varepsilon=10^{-3}$ (DLR).

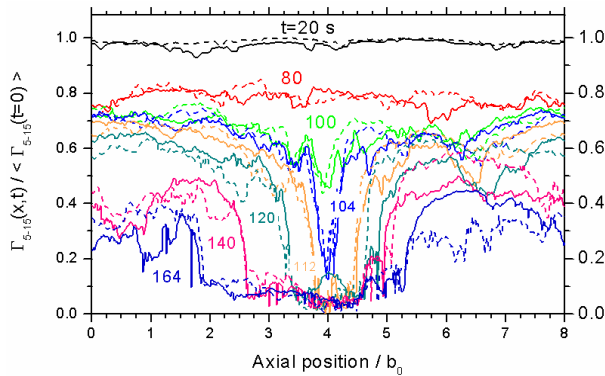


FIG 27. As Fig. 26, but showing variation of circulation strengths along the length of the computational box.

5. THE FLIGHT TESTS

The first flight tests were performed quite early in the project in August 2003. Two smoke generators were mounted underneath the wings to enable a visualisation of the wake from the NLR Citation aircraft flying about 1500 ft below. At that time, based on an assessment made at the start of the project, the use of an on-board LIDAR technique to measure the wakes was considered too risky and therefore wake measurements were made with ground based continuous wave (CW) LIDAR's from ONERA and DLR (applying a triangulation method) and also with an additional pulsed LIDAR from DLR. The test set-up is shown in Fig. 28.

A detailed discussion of F/T-1 LIDAR measurements is given in [11]. The baseline and an in- and outboard loaded differential spoiler setting (yielding only a relatively mild change in wing span-loading) were tested. No significant effect of aircraft configuration on the wake decay could be observed. Instead the observed wake decay was predominantly influenced by the atmospheric turbulence level, very similarly as during tests with the baseline A340-300 configuration made in the C-Wake project (see Fig. 29).

Furthermore, flow visualisations taken at a higher altitude in low-atmospheric turbulence conditions did not show a significant difference between the configurations (see Fig. 30 for $\varepsilon \approx 2.10^{-5}$). The vortex linking process appears only completed after about 8 NM. The development of Crow modes (leading to vortex linking) and various vortex "bursting" phenomena are visible. All configurations tested during F/T-1 show similar results.

Following a successful application of the DLR pulsed LIDAR during F/T-1, a try-out flight test with the pulsed LIDAR on-board a Falcon aircraft was made by DLR. Based on the excellent results [12], the on-board LIDAR test technique was selected for F/T-2, enabling a simultaneous visualisation and measurement of the wake.

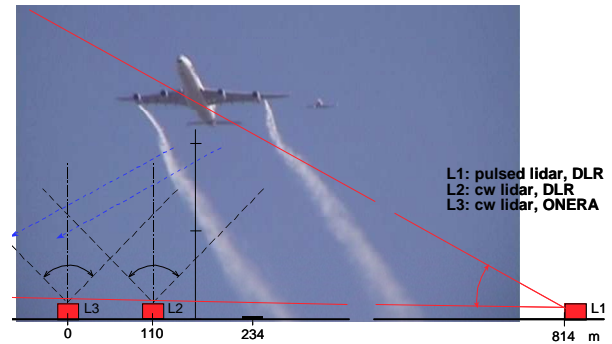


FIG 28. Ground based LIDAR test setup for F/T-1. L1: Pulsed LIDAR (DLR); L2/L3: CW-LIDAR's from DLR/ONERA.

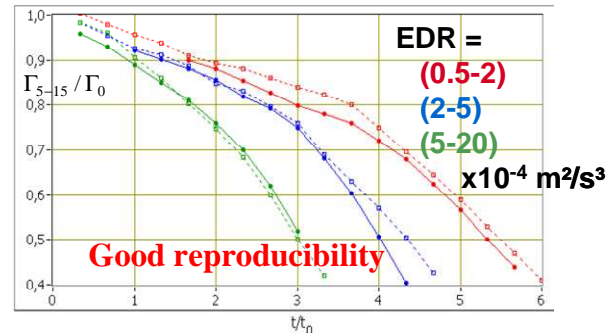


FIG 29. Average wake decay depending on atmospheric turbulence class (DLR). Broken lines: Awiatore F/T-1 (2003, 3 different configurations). Full lines: C-Wake (2002, baseline configuration).

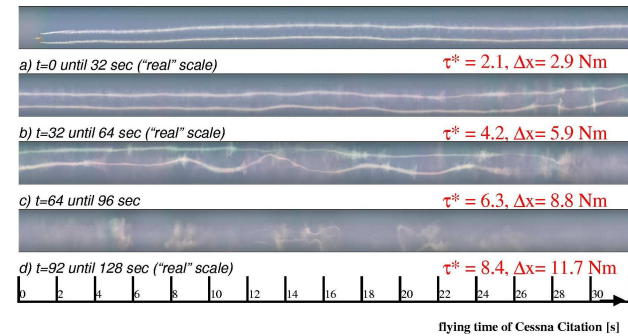


FIG 30. Example of wake visualisation (stitched video) of smoke traces recorded from NLR chase plane (F/T-1).

During F/T-2, the DFS 32/10 configuration was tested in relatively calm air. Nevertheless, vortex linking occurred earlier than for all other configurations tested in more turbulent conditions at Nov. 15. This already shows the benefits of the DFS 32/10 configuration. Also, the first observed vortex linking for DFS 32/10 occurred quicker than during the baseline tests in F/T-1. DFS 32/10 shows on average (see Fig. 31) about 20 % earlier vortex linking, which is consistent with the smaller time scale t_0 (see chapter 1) to be expected from the observed 6% reduction in vortex spacing. Atmospheric turbulence was measured with the nose-booms from the NLR Metro and DLR

Falcon aircraft and evaluated with a structure function approach. Considering the variation in actual atmospheric turbulence levels along the flight paths and the variation with altitude (up to about 2 orders of magnitude, as shown in [3]), these results need to be interpreted with some caution. The LIDAR measurements provide additional quantitative information. The measured wake decay during F/T-2 for the different configurations is shown in Fig. 32. The symbols indicate individual data points, the lines are time window averaged values per configuration. On average, the DFS 32/10 case shows somewhat faster decay than the baseline configuration, despite the fact that the atmospheric turbulence during these measurements was lower. For equal wake vortex strength the difference in non-dimensional time corresponds to about 0.5 time units.

Assuming that wake decay is governed by a 2-phase wake decay model (such as the deterministic version of the DLR P2P model), IRPHE proposed a method [3] that shifts individual measurements by $\Delta\tau^*$, depending on the turbulence level ε . Corrected results more clearly show the benefits of the DFS 32/10 configuration (see Fig. 33).

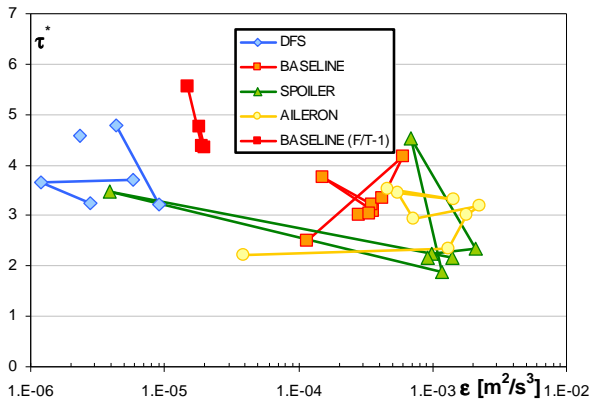


FIG 31. Vortex linking time τ_v from smoke visualisations (NLR: F/T-2), shown as function of the average eddy dissipation rate ε . Results for F/T-1 baseline configuration are added for comparison.

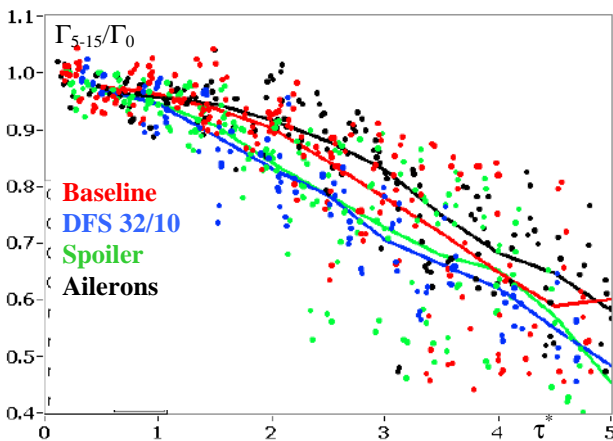


FIG 32. Vortex decay from LIDAR measurements for all configurations tested during F/T-2 (tested in different atmospheric turbulence conditions by Airbus and DLR).

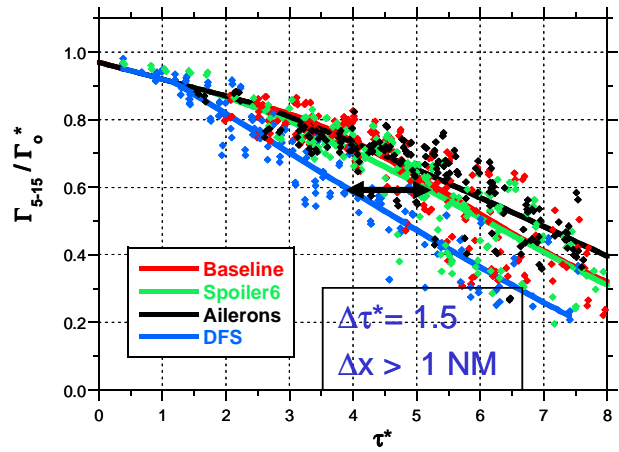


FIG 33. Vortex decay after applying correction procedure for atmospheric turbulence from IRPHE. All individual results are corrected to a common low ($\varepsilon^* = 0.05$) atmospheric turbulence level.

6. CONCLUSIONS

The combined theoretical, numerical and experimental work performed in the AWIATOR wake vortex task has much improved the physical understanding of the complex processes that play a role in the formation, roll-up, merging, instability growth mechanisms, and final decay characteristics of wake vortices. The results were used for the selection of promising flight test configurations.

The work led to significant improvements in wake measurement techniques:

- Improved understanding of towing tank test performance, including awareness of possible vertical stratification and end effects, in comparison to wind tunnel and F/T results.
- Mitigation of end effects in the B20 catapult facility by optimum placement of observation plane with respect to model launching and model recovery box.
- The development and successful use of a mini-LIDAR in B20 catapult facility.
- The application of a hot-wire sensor for scanning the wake to determine both the mean flow as well as the flow turbulence characteristics in the wake was very valuable to check possible near wake instabilities.
- The use of smoke generators in flight tests, leading to a much improved signal-to-noise ratio for the LIDAR signals and to the possibility to visualise the wake vortices.
- A successful try-out test with a unique on-board pulsed LIDAR measuring technique.
- Successful application of the on-board pulsed LIDAR technique during the second flight test campaign.
- The development of an efficient flight testing procedure with wake monitoring aircraft and on-board pulsed LIDAR.

The work also led to significant progress in CFD applications, in particular:

- Challenging RANS simulations of a high-lift configuration with resolved vortices in the near wake.
- The application of simple numerical methods:
 - 2D vortex methods for near-wake vortex topology calculations, starting from design span loading distributions.
 - 2D viscous methods, tuned to experimental

results, for improved wake roll-up simulations up to extended near-wake.

- The application of advanced LES methods:
 - 2D temporal LES simulations starting from experimental data in the near wake.
 - A detailed comparison of four numerical methods in a benchmark simulation exercise.
 - 3D temporal LES simulations for simulating the effect of atmospheric turbulence on wake decay, helped to understand the observed scatter in LIDAR measurements.
 - 3D temporal LES simulation of oscillating ailerons, starting from given span-loading distributions. Based on these simulations the oscillating aileron case was selected for F/T-2.
 - 3D temporal LES simulations of wake vortex merging and roll-up showed for the DFS 32/10 case a distinct, more violent, interaction of the vortices during merging, producing additional turbulence around the main vortex.

Regarding the results of the flight tests and the effectiveness of the investigated wing modifications the following conclusions are made:

- The DFS32/10 configuration was measured during F/T-2 in relatively low atmospheric turbulence conditions. From the flow visualisations the time to vortex linking was found to be reduced by about 20% compared to the baseline configuration tested in equally low turbulence during F/T-1. This is consistent with the observed 6% reduction in vortex spacing for this configuration.
- During F/T-2 all other configurations were tested in more turbulent conditions and therefore the LIDAR data show a considerable scatter in measured circulation strengths.
- This is in good qualitative agreement with numerical simulation results on the effect of turbulence on wake decay, showing large variations in 3D deformation of vortex lines due to atmospheric turbulence effects.
- For each configuration tested in F/T-2 eight wake developments were measured. More measurements would have improved the statistical reliability.
- An interesting procedure to correct for atmospheric turbulence effects was proposed by IRPHE. It assumes wake decay can be modelled by a two-phase decay model. Results are corrected by applying a time-shift correction $\Delta\tau^*$, depending on the atmospheric turbulence level.
- After correction the DFS 32/10 configuration shows even more rapid wake decay compared to the other configurations tested.
- Although the DFS 32/10 and the spoiler #6 configuration have about equal lateral vortex spacing they display different decay behaviour. In LES simulations the vortex merging process of the DFS 32/10 configuration is seen to produce more turbulence around the vortices. This might explain the different decay behaviour.
- Based on the F/T results and acknowledging the differences in atmospheric turbulence the benefits for the DFS 32/10 configuration are estimated to be quite significant: up to about 1 NM separation distance.

Concluding remarks

The present paper gives a summary of the work performed in the AWIATOR wake vortex task. Some other results will be dealt with in the accompanying paper [3].

Acknowledgement

This work was done in a collaborative research project, co-funded by the European Commission under the 5th Framework. The support of the European Commission is highly appreciated. Contributions to the work were (amongst others) given by: K. Schröder, F. Laporte, A. Namer, E. Delfieu (Airbus); E. Coustols, A. Dolfi-Bouteyre, F. Moens, L. Jacquin (ONERA); Th. Gerz, R. Baumann, S. Rahm, F. Köpp, I. Smalikho, S. Melber, H. Vollmers, C. Carmer (DLR); A. Elsenaar, A. Karwal, H. Kannemans, G. van Baren (NLR); G. Winckelmans, L. Dufresne, R. Capart, O. Desenfans (UCL); L. Nybelen, J. Boussuge, H. Moet (CERFACS); C. Breitsamter, C. Bellastrada (TUM-AER); Th. Leweke (IRPHE), J. Pereira (IST).

7. REFERENCES

- [1] G. Schrauf; F. Laporte: AWIATOR wake-vortex characterization methodology, KATnet Conference on key Aerodynamic Technologies, 20-22 June 2005, Bremen (also presented at AIAA conference Reno, Jan 2006)
- [2] A.C. de Bruin: AWIATOR, Task11 Wake Vortex, Wake alleviation by design, Wakenet Europe Workshop 2007, Eurocontrol, Haren, Belgium, 5-7 February, 2007.
- [3] J. König, A.C. de Bruin: Requirements and results of wake vortex in-flight measurements in AWIATOR, CEAS, Berlin, September 10-13, 2007.
- [4] T. Gerz, F. Holzäpfel, D. Darracq: Commercial aircraft wake vortices, Progress in Aerospace Sciences, 38, 181-208, 2002.
- [5] V.J. Rossow: Lift-generated vortex wakes of subsonic transport aircraft, progress in Aerospace sciences 35 (1999) 507-660.
- [6] F. Holzäpfel, T. Gerz, F. Köpp, E. Stumpf, M. Harris, R.I. Young, A. Dolfi-Bouteyre: Strategies for circulation evaluation of aircraft wake vortices measured by lidar, J. Atmos. Ocen. Tech., Vol. 20, No. 8, 1183-1195, 2003.
- [7] J.M. Ortega, R.L. Bristol, O. Savas: Experimental study of the instability on unequal-strength counter-rotating vortex pairs. JFM, 474, 35-84, 2003.
- [8] C. Bellastrada; C. Breitsamter: Effect of differential flap settings on wake vortex evolution of large transport aircraft. In: Notes on Numerical Fluids Mechanics, New Results in Numerical and Experimental Fluid Mechanics V, 14th AG STAB/DGLR Symposium, Bremen, 2004, (NNFM) Vol. 92, Springer Verlag, 2006.
- [9] Dolfi-Bouteyre; J.-P. Cariou; D. Fleury; D. Goular; J.-P. Lafforgue: Measurement of Aircraft Wake Vortex using Coherent Laser Radar, Comparison between catapult and airport measurements, CLRC13 Conference, Oct 2005, Japan.
- [10] Th. Gerz; R. Baumann: Decay characteristics of single and double wake-vortex pairs in different atmospheric flow realisations, presented at the 25. Congress of ICAS, 4-8 September 2006, Hamburg.
- [11] F. Köpp; S. Rahm; I. Smalikho; A. Dolfi; J.-P. Cariou; M. Harris: Comparison of Wake-Vortex parameters measured by pulsed and continuous wave lidars, Journal of Aircraft 2005, Vol.42 no.4 (916-923).
- [12] S. Rahm; I. Smalikho; F. Köpp: Characterisation of aircraft wake vortices by airborne coherent doppler lidar, Journal of Aircraft, to appear in Vol. 44, 2007.